High spin spectroscopy of ^{201}Tl

S. Das Gupta,[1] S. Bhattacharyya,[1,*] H. Pai,[1,†] G. Mukherjee,[1] Soumik Bhattacharya,[1] R. Palit,[2] A. Shrivastava,[3] A. Chatterjee,[3] S. Chanda,[4] V. Nanal,[2] S. K. Pandit,[3] S. Saha,[2] J. Sethi,[2] and S. Thakur[2]

[1]*Variable Energy Cyclotron Centre, 1/AF Bidhannagar, Kolkata 700064, India*

[2]*Department of Nuclear and Atomic Physics, Tata Institute of Fundamental Research, Mumbai 400005, India*

[3]*Nuclear Physics Division, Bhabha Atomic Research Centre, Mumbai 400085, India*

[4]*Fakir Chand College, Diamond Harbour, West Bengal, India*

(Received 24 July 2013; revised manuscript received 12 September 2013; published 25 October 2013)

The high spin structure of ^{201}Tl has been studied by γ-ray spectroscopic method using the ^{198}Pt(^{7}Li,4n)^{201}Tl reaction at 45 MeV beam energy. The level scheme of ^{201}Tl has been considerably extended through the observation of 31 new transitions. Several new band structures have been established. The $9/2^-$ oblate band has been significantly extended beyond the particle alignment frequencies. The band structures and the other excited states have been compared with the neighboring odd-A Tl isotopes and with the even-even core nucleus ^{200}Hg. The total Routhian surface calculations have been performed to study the deformation and shape changes as a function of spin in this nucleus.

DOI: 10.1103/PhysRevC.88.044328 PACS number(s): 21.10.−k, 23.20.Lv, 23.20.En, 27.80.+w

I. INTRODUCTION

Thallium isotopes in the mass 190–200 region with only one proton hole and a few neutron holes outside the ^{208}Pb doubly magic ($Z = 82$ and $N = 126$) core are expected to have spherical structure. On the other hand, they can also be characterized by a single proton particle outside the $Z = 80$ deformed even-even core of corresponding Hg isotopes. This has generated a great deal of interest in understanding the underlying angular momentum coupling schemes and the interplay of the valence particle with the collective degrees of freedom of the core, below $Z = 82$ [1–3]. Variation of the nuclear deformation as a function of angular momentum for the chain of Tl isotopes makes them interesting candidates to test the predictions of different theoretical models and their validity at high spin and excitation. A variety of shapes and structures have been observed in the odd-A Tl isotopic chain, ranging from the strongly coupled weakly deformed oblate band structure in ^{191,193,195,197,201}Tl [4–7], to the superdeformed structure in neutron deficient ^{191,193,195}Tl [8–10], and the recently observed octupole core excitation in neutron-rich ^{205}Tl [11]. The deformation driving intruder proton $h_{9/2}$ and $i_{13/2}$ orbitals are mainly responsible for the collective band structures in these nuclei. The heavier Tl isotopes, close to ^{208}Pb, are expected to have spherical structure at lower excitation while the deformation may set in for higher spin states. For odd-A Tl isotopes the ground state spin is 1/2, corresponding to the occupation of the $s_{1/2}$ orbital below the $Z = 82$ spherical core. The intruder $\pi h_{9/2}$ orbital above the $Z = 82$ shell closure is accessible by the odd proton in the case of oblate deformation. A rotational oblate band built on the $9/2^-$ isomeric level has been reported systematically for all odd-mass Tl isotopes [12], with only a few members of this band identified in ^{201}Tl [13]. It would be interesting to investigate whether and how far the oblate deformation persists at higher spin for the heavier Tl nuclei as the neutron number approaches the closed shell of $N = 126$.

Prior to the present work, there were no high spin data on ^{201}Tl from heavy-ion-induced reactions, mainly due to the limited options for target-projectile combination available to access the heavier isotopes of Tl. The previous study on ^{201}Tl used a deuteron-induced fusion reaction [13], and a few γ rays belonging to the higher spin members were only tentatively placed, using one coaxial and two planer Ge(Li) detectors. Due to a lesser degree of alignment in such a light-ion-induced reaction, unambiguous spin-parity assignment was difficult from angular distribution data for most of the higher excited states observed in Ref. [13]. Rotational bands based on the intruder $\pi i_{13/2}$ orbital have been observed in some of the lighter odd-mass Tl nuclei [6,13] and recently in ^{197}Tl [14], but not yet identified in heavier Tl isotopes. The aim of the present work is to extend the yrast and non-yrast band structures of ^{201}Tl to higher spin states with definite spin and parity assignments.

II. EXPERIMENT AND ANALYSIS

The high spin states in ^{201}Tl have been populated by the fusion-evaporation reaction ^{198}Pt(^{7}Li,4n) at a beam energy of 45 MeV, obtained from the BARC-TIFR Pelletron LINAC facility at Mumbai, India. A 1.3 mg/cm^2 thick ^{198}Pt self-supporting foil with 95.7% enrichment was used as a target. At the beam energy of 45 MeV, 4n and 5n channels were found to be the dominant fusion evaporation channels. However, due to the weakly bound nature and various cluster structure configurations of the ^{7}Li beam, in addition to complete fusion, incomplete fusion (i.e., the capture of one of the fragments of the cluster by the target nuclei) channels also make a significant contribution to the reaction process. The cross sections for complete fusion and capture of various cluster fragments were measured in a separate experiment [15]. The Indian National Gamma Array (INGA), configured with 15

*Corresponding author: sarmi@vecc.gov.in

†Present address: Institut für Kernphysik, Technische Universität Darmstadt, D-64289 Darmstadt, Germany.

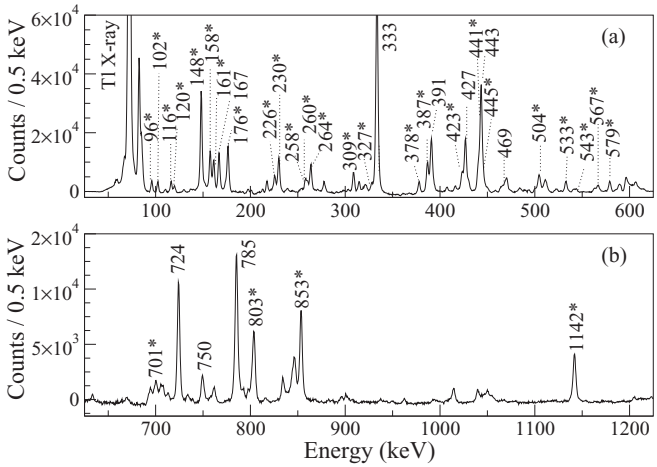

FIG. 1. Coincidence spectra by gating on the 319 keV γ transition. (a) The lower energy part and (b) the higher energy part of the spectrum. The new peaks observed in the present work are marked with "$*$".

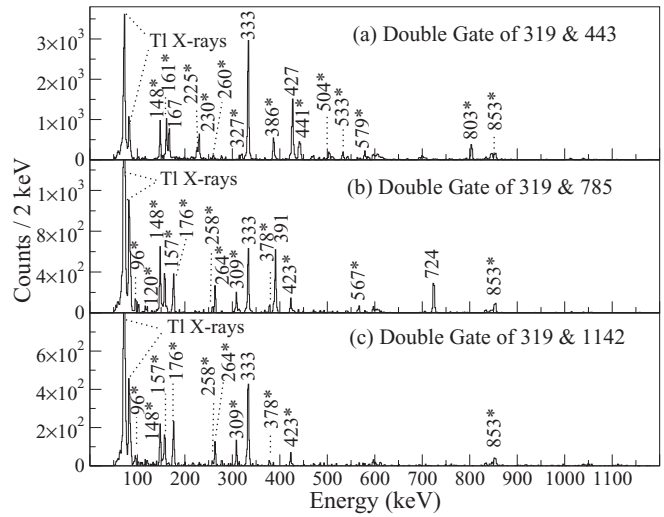

FIG. 2. Coincidence spectra corresponding to double gates of (a) 319 and 443 keV, (b) 319 and 785 keV, (c) 319 and 1142 keV pertaining to the two separate cascades of transitions in ^{201}Tl.

Compton suppressed clover high purity germanium (HPGe) detectors, was used to detect the γ rays in coincidence. In this particular array configuration, the detectors were arranged in six different angles with two detectors each at $\pm 40^\circ$ and $\pm 65^\circ$ while four detectors were at 90° and three were at -23°. The time stamped data were collected using a digital data acquisition system with a sampling rate of 100 MHz. Further details of this data acquisition system can be found in Ref. [16]. The coincidence events in which at least two clover detectors have fired were selected for the analysis. The energy calibration and efficiency of each detector were obtained with ^{133}Ba and ^{152}Eu standard sources. The raw data were sorted using the MultipARameter time-stamp based COincidence Search (MARCOS) sorting program, developed at the Tata Institute of Fundamental Research (TIFR), Mumbai, to generate the γ-γ matrix and γ-γ-γ cube, after gain-matching the energy of each clover detector to 0.5 keV/channel and 2 kev/channel respectively. A coincidence time window of 400 ns was selected to generate the above matrix and the cube. Further, various coincidence time windows from 50 ns to 1 μs were set to generate different γ-γ matrices to check for the presence of any delayed component.

A representative coincidence spectrum corresponding to a gate at 319 keV, obtained from the γ-γ matrix, is shown in Fig. 1. Figures 2, 3, and 4 represent typical double-gated spectra corresponding to different cascades of γ rays, as obtained from the γ-γ-γ cube. To extract the coincidence relationship between various γ-transitions, the analysis of the γ-γ matrix and γ-γ-γ cube were carried out using RADWARE [17] and INGASORT [18] analysis packages. The coincidence spectrum shown in Fig. 1 corresponds to the gate on the lowest transition of the $9/2^-$ band. Most of the new transitions can be identified from this coincidence spectrum. The total gamma spectrum was found to be of complex nature, due to the contribution of both complete fusion and different incomplete fusion channels, producing Tl and nearby nuclei having similar γ transitions. Therefore, for most of the cases, the coincidence relationships were mainly obtained from the double-gated spectra generated from the γ-γ-γ cube. The origin of various transitions known from the previous experiment of particle-γ coincidence [15] was also used as a guide for assignments of γ rays to a particular nucleus.

The information on the multipolarity of the γ rays was obtained from the analysis of the ratio of directional correlation from oriented states (DCO) [19], for which an asymmetric γ-γ matrix, with x axis containing the data from the -23° (θ_1) detectors and y axis containing the data from the 90° (θ_2) detectors, was generated. The DCO ratio of a transition (γ_1) is then obtained from the ratio of its intensities at two angles θ_1 and θ_2 gated by another transition (γ_2) of known multipolarity, as per the following expression:

$$R_{\mathrm{DCO}} = \frac{I_{\gamma_1} \text{ at } \theta_2, \text{ gated by } \gamma_2 \text{ at } \theta_1}{I_{\gamma_1} \text{ at } \theta_1, \text{ gated by } \gamma_2 \text{ at } \theta_2}. \quad (1)$$

For a pure stretched quadrupole or dipole transition, the R_{DCO} should be close to unity gated by a transition of

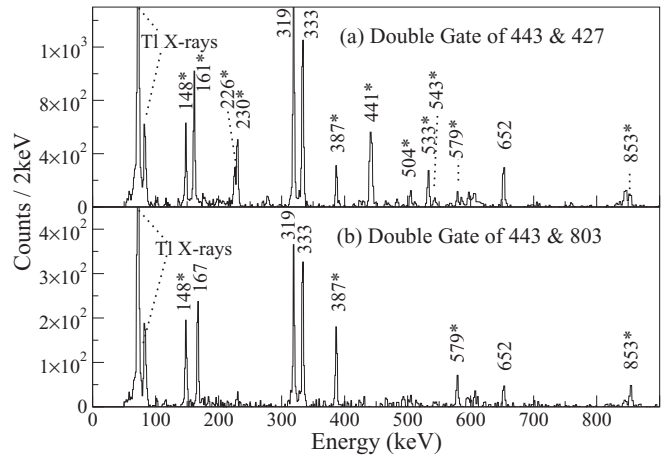

FIG. 3. Coincidence spectra corresponding to double gates of (a) 443 and 427 keV, (b) 443 and 803 keV, corresponding to the transitions in ^{201}Tl.

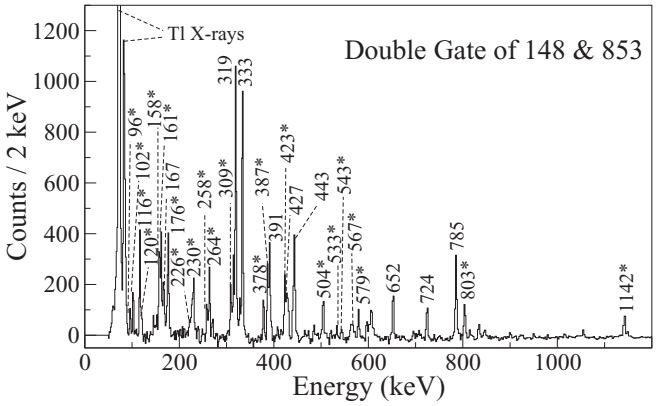

FIG. 4. Coincidence spectra corresponding to double gates of 148 and 853 keV transitions in ^{201}Tl.

same multipolarity. For the gating transition of different multipolarities, the R_{DCO} value depends on the nature of the gating transition. In the present analysis, the typical values of R_{DCO} for a dipole gate comes out to be $\sim$ 1.0 for pure dipole transitions and $\sim$ 0.5 for pure quadrupole transitions. For a quadrupole gate, the values are found to be $\sim$ 2.0 and $\sim$ 1.0 for pure dipole and quadrupole transitions, respectively. These values are corroborated by the analysis of known $E2$ and $M1$ transitions in ^{201}Tl and the transitions of neighboring isotopes of Tl, Hg, and Au, populated in the same reaction. For example, the DCO ratios of the 659 keV ($E2$) and 132 keV ($M1$) transitions in ^{200}Tl come out as 0.52(3)and 0.97(4), respectively, when gated by the known dipole transition of 119 keV. From the 659 keV quadrupole gate, the DCO ratio of the 119 keV ($M1$) γ transition comes out as 2.1(4). On the other hand, in the quadrupole gate of 368 keV gamma ray in ^{200}Hg, the R_{DCO} value for the 579 keV quadrupole transition was obtained as 1.18(1). The multipolarities of various transitions in ^{201}Tl are obtained from the deduced DCO ratios either from the known quadrupole gate of 652 keV or the gate of the other deduced dipole or quadrupole transitions, as shown in Fig. 5.

The parities of most of the excited states could be assigned from the polarization measurement by exploiting the close configuration of the four Ge crystals in the clover Ge detector. The information regarding the type (electric or magnetic) of the transitions is obtained from the integrated polarization directional correlation (IPDCO) asymmetry parameter following the prescription of Refs. [20,21]. This was deduced from the parallel and perpendicular scattering components of a γ ray incident on a clover detector. The detectors placed at 90° in the INGA array were used for this. The IPDCO asymmetry parameter is defined as,

$$\Delta_{IPDCO} = \frac{a(E_\gamma)N_\perp - N_\parallel}{a(E_\gamma)N_\perp + N_\parallel}, \qquad (2)$$

where $N_\parallel$ and $N_\perp$ are the number of counts corresponding to the parallel and perpendicular Compton scattered components of a γ ray in the planes parallel and perpendicular to the reaction plane, respectively. $a(E_\gamma)$ is the correction factor due to any geometrical asymmetry of the detector array or asymmetry in the response of the four crystals of a clover Ge detector. This factor is defined as $a(E_\gamma) = N_\parallel/N_\perp$ and

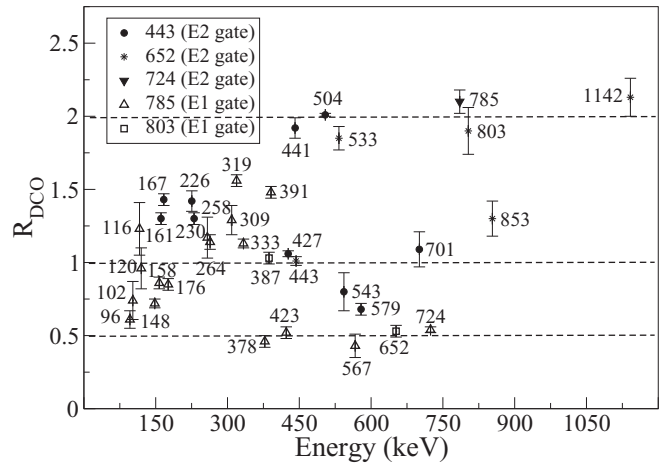

FIG. 5. DCO ratios of various transitions in ^{201}Tl obtained with different dipole or quadrupole gates as indicated. The dotted lines at 0.5, 1.0, and 2.0 correspond to the values for a quadrupole transition in a pure dipole gate, for a transition of same multipolarity as the gated transition, and for a dipole transition in a pure quadrupole gate, respectively, and are shown to guide the eye.

can be obtained using scattered components of γ rays from an unpolarized source, which should be close to unity. For the present setup, this correction factor (a_{γ_0}) was obtained as 1.037(37) from the fitting of its variation as a function of γ-ray energy, using ^{133}Ba and ^{152}Eu radioactive sources, as shown in Fig. 6. In order to extract the parallel and perpendicular scattered components of a transition, two asymmetric E_γ-E_γ matrices corresponding to parallel and perpendicular segments of the clover detectors at 90° along one axis and the coincident γ rays from the other detectors along another axis were constructed. From the projected spectra of the above matrices, the number of perpendicular ($N_\perp$) and parallel ($N_\parallel$) scatterers for a given γ ray could be obtained. Using the fitted parameter a_{γ_0}, the Δ_{IPDCO} for most of the γ rays in ^{201}Tl have been determined. A positive value of Δ_{IPDCO} means that the transition is electric whereas a negative value confirms a magnetic transition. Again, the nature of the known transitions in ^{200}Tl,^{199,200}Hg, and ^{198,199}Au nuclei, which

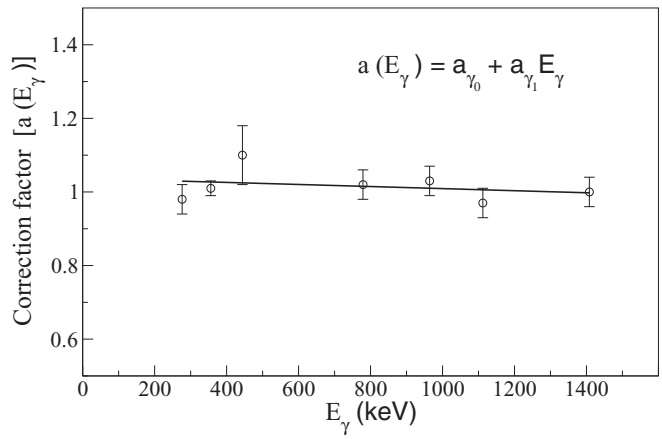

FIG. 6. The asymmetry correction factor $a(E_\gamma)$ as a function of γ-ray energies from standard sources.

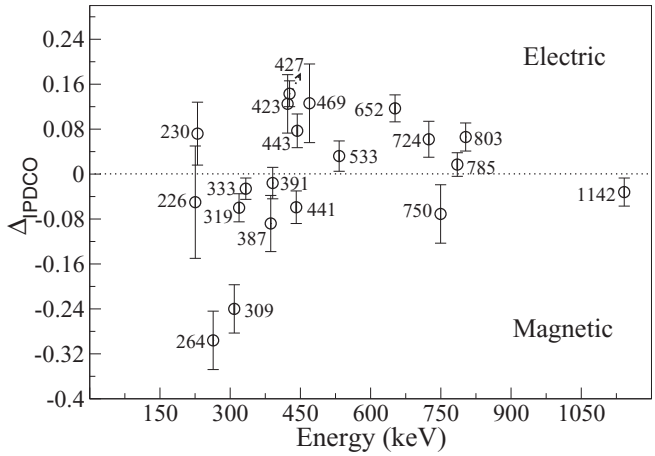

FIG. 7. IPDCO ratios of various transitions in ^{201}Tl obtained in the present work. The dotted line indicated at $\Delta_{IPDCO} = 0$ is drawn to show the electric and magnetic transitions at positive and negative sides of this value respectively.

were also produced in our experiment, could be reproduced from the deduced Δ_{IPDCO}, to check the consistency of our polarization analysis. The Δ_{IPDCO} analysis for ^{194}Tl, using the same detector array setup, produced in a different reaction has been reported earlier [22]. The deduced Δ_{IPDCO} values for various transitions in ^{201}Tl are shown in Fig. 7.

III. RESULTS

The energies and intensities of the observed γ rays from the present work, which are placed in the level scheme of ^{201}Tl, have been tabulated along with other relevant quantities in Table I. Figure 8 represents the proposed level scheme of ^{201}Tl, above the $9/2^-$ isomer, obtained from the present work. The present level scheme indicates a significant extension of the main band built on the $9/2^-$ isomeric level compared to earlier work [13], as well as the observation of several other cascade of transitions to higher spins. The construction of the level scheme of ^{201}Tl is based on coincidence relations of identified transitions, intensity balance, DCO, and polarization measurement. A total of 31 new transitions in ^{201}Tl have been identified and most of them are placed in the level scheme, which are marked with asterisks in Fig. 8. The relative intensities of the γ rays have been deduced from both the total projection of the γ-γ matrix and the gated spectra after correcting for the detector efficiencies.

Several new side branches and bandlike sequences have been established from the present work other than the extension of the band built on the $9/2^-$ isomer. Moreover, the 167, 427, 469, 750, and 785 keV transitions, which were tentatively assigned in the previous work [13], have been confirmed from the present measurements. Figures 2(a), 2(b), and 2(c) show the spectra corresponding to double gates of 319 and 443 keV, 319 and 785 keV and 319 and 1142 keV, respectively. From these spectra, it is clear that a separate set of transitions, leading to sequence B, are connected to the main band by the 785 keV transition at the 1963 keV $(15/2^-)$ level. The 785 keV γ ray was found to be an $E1$ type transition from the DCO ratio and IPDCO analysis, making the spin-parity of 2748 keV level $17/2^+$. The spin-parities of all the states above 2748 keV were assigned from the deduced DCO ratios and Δ_{IPDCO} values based on the 785 keV gate. The Δ_{IPDCO} values for the 264 and 309 keV transitions were obtained from the sum gate of 319, 391, 652, 724, 785, and 1142 keV transitions. The Δ_{IPDCO} of the 423 keV γ ray comes out as positive, deduced from the sum gate of 785 and 1142 keV to avoid the contribution of the 427 keV transition. That, together with the quadrupole nature of this transition obtained from the DCO ratio, makes it an $E2$ transition. The Δ_{IPDCO} values for the 258 and 567 keV γ rays could not be obtained due to the lack of statistics, but the DCO ratio of the 258 keV transition could be deduced and is attributed as a mixed, $M1 + E2$ transition. Since the 567 keV is a crossover transition of mixed 258 and 309 keV transitions, it is considered to be an $E2$ transition.

Two separate cascades of 309–258–120 keV and 264–423 keV have been established on top of the 2748 keV level on the basis of the coincidence relationship between these cascades with the other lower lying transitions. The spin-parity of the 3435 keV level is fixed from the deduced DCO ratio and Δ_{IPDCO} of both 378 and 423 keV transitions. For the low energy transitions of 96, 120, 158, and 176 keV, the IPDCO analysis was not possible due to low scattering probability, but from their deduced DCO ratios they are found to be of mixed multipolarity.

The 1572 keV $(13/2^-)$ level of the main band is also fed by an $M1$ transition of 1142 keV. The $M1$ nature of the 1142 keV transition is established from the DCO ratio obtained from the 652 keV quadrupole gate and Δ_{IPDCO} from the sum gate of 319 and 652 keV. Figure 2(c) shows a double-gated spectrum corresponding to the 319–1142 keV cascade. The absence of the 391 keV transition but the presence of the 333 keV transition at this gate fixes the placement of 1142 keV transition in the level scheme, connecting it to the main sequence (A) at the 1572 keV level. It is also clear from the above spectrum that the set of γ rays above the 2748 keV level are also in coincidence with the 1142 keV transition. This establishes the presence of a connecting transition of 34 keV of $E1$ nature between the 2748 keV and the 2714 keV levels which is consistent with the theoretical Weisskopf estimate [23] of the half-life ($\sim$ 5.14 ps) of the 2748 keV level. The low energy threshold of the experimental setup did not allow this transition to be observed in the present work.

Figure 3(a) and 3(b) show the spectra corresponding to the double gates of 443 and 427 keV and of 443 and 803 keV cascades, respectively. From these two spectra it is clear that 427 and 803 keV are parallel to each other, leading to the sequences C and D, respectively, and are both connected to the $9/2^-$ band through 443 keV γ ray. The presence of the 427 keV line in the spectrum gated by 391 keV γ ray and also the presence of all the lower and higher lying lines in the double-gated spectrum of the 391 and 427 keV γ rays indicates that the 2015 and 1963 keV levels are connected by a small 52 keV transition. This connecting transition could not be detected in our experiment due to its high conversion probability and small detection efficiency at this γ-ray energy. The 443 keV γ ray was found to be of quadrupole nature from

TABLE I. The energy (E_γ) and intensity (I_γ) of the γ rays placed in the level scheme of ^{201}Tl along with the spin and parity of the initial (J_i^π) and the final (J_f^π) states and the energy of the initial state (E_i). The measured values of R_{DCO} and Δ_{IPDCO} are also shown along with the proposed multipolarity of the γ rays.

E_γ (keV)	E_i (keV)	$J_i^\pi \rightarrow J_f^\pi$	I_γ[a]	R_{DCO}(Err)	Δ_{IPDCO}(Err)	Deduced multipolarity
96.1(1)	3530.9	$25/2 \rightarrow 23/2^+$	1.95(3)	0.61(6)[b]		$(M1+E2)$
119.8(2)	3434.8	$23/2^+ \rightarrow 21/2^+$	1.51(35)	0.96(14)[b]		$M1$
157.5(1)	3864.6	$29/2 \rightarrow 27/2$	7.62(71)	0.86(4)[b]		$M1+E2$
161.2(1)	3044.6	$25/2^- \rightarrow 23/2^-$	6.08(71)	1.30(4)[c]		$M1+E2$
166.9(1)	2182.2	$19/2^- \rightarrow 17/2^-$	7.53(69)	1.43(4)[c]		$M1+E2$
176.2(1)	3707.1	$27/2 \rightarrow 25/2$	10.94(83)	0.85(4)[b]		$M1+E2$
211.8(2)	2883.4	$23/2^- \rightarrow 23/2^+$	0.70(15)			$(E1)$
225.5(1)	2898.0	$25/2^+ \rightarrow 23/2^+$	3.98(58)	1.42(7)[c]	−0.05(10)	$M1+E2$
230.2(1)	2672.5	$23/2^+ \rightarrow 21/2^-$	9.04(69)	1.30(4)[c]	0.072(56)	$E1$
258.0(1)	3315.0	$21/2^+ \rightarrow 19/2^+$	2.4(12)	1.17(14)[b]		$M1+E2$
260.1(1)	2442.3	$21/2^- \rightarrow 19/2^-$	2.2(12)			$(M1)$
263.7(1)	3011.9	$19/2^+ \rightarrow 17/2^+$	7.24(66)	1.14(5)[b]	−0.296(52)	$M1$
308.8(9)	3057.0	$19/2^+ \rightarrow 17/2^+$	5.61(55)	1.29(10)[b]	−0.240(43)	$M1+E2$
319.0(1)	1238.6	$11/2^- \rightarrow 9/2^-$	100.0(58)	1.56(4)[b]	−0.060(25)	$M1+E2$
326.7(3)	3372.0	$23/2^+ \rightarrow 25/2^-$	2.38(53)			$(E1)$
333.4(1)	1572.0	$13/2^- \rightarrow 11/2^-$	75.3(35)	1.13(3)[b]	−0.026(19)	$M1$
377.9(1)	3434.8	$23/2^+ \rightarrow 19/2^+$	3.93(44)	0.46(4)[b]		$E2$
386.8(1)	3431.4	$27/2^- \rightarrow 25/2^-$	4.65(26)			$(M1+E2)$
386.7(1)	3371.3	$23/2^+ \rightarrow 21/2^+$	5.41(76)	1.03(4)[d]	−0.088(50)	$M1$
390.9(1)	1963.0	$15/2^- \rightarrow 13/2^-$	22.9(14)	1.48(4)[b]	−0.016(28)	$M1+E2$
422.8(2)	3434.8	$23/2^+ \rightarrow 19/2^+$	4.19(78)	0.52(4)[b]	0.125(52)	$E2$
426.8(1)	2442.3	$21/2^- \rightarrow 17/2^-$	24.0(15)	1.06(2)[c]	0.143(23)	$E2$
441.1(7)	2883.4	$23/2^- \rightarrow 21/2^-$	6.8(26)	1.92(7)[c]	−0.059(29)	$M1$
443.3(8)	2015.3	$17/2^- \rightarrow 13/2^-$	47.1(39)	1.01(3)[e]	0.077(30)	$E2$
445.2(7)	2486.6	$(17/2) \rightarrow 15/2^+$	6.28(72)	0.71(5)[f]		
469.4(2)	2041.4	$15/2^+ \rightarrow 13/2^-$	11.02(84)	1.80(67)[e]	0.126(70)	$E1$
504.4(1)	3935.8	$29/2 \rightarrow 27/2^-$	6.5(10)	2.01(1)[c]		$M1/E1$
532.8(1)	3431.4	$27/2^- \rightarrow 25/2^+$	4.92(46)	1.85(8)[c]	0.032(27)	$E1$
543.2(4)	2985.3	$21/2^+ \rightarrow 21/2^-$	1.40(41)			$E1$
566.8(3)	3315.0	$21/2^+ \rightarrow 17/2^+$	4.22(50)	0.43(8)[b]		$E2$
579.1(1)	3951.0	$(25/2^+) \rightarrow 23/2^+$	4.83(45)	0.68(4)[c]		$(M1+E2)$
652.2(5)	1572.0	$13/2^- \rightarrow 9/2^-$	32.9(24)	0.53(4)[d]	0.117(24)	$E2$
700.9(3)	2883.4	$23/2^- \rightarrow 19/2^-$	1.77(59)	1.09(12)[c]		$E2$
724.3(1)	1963.0	$15/2^- \rightarrow 11/2^-$	20.2(17)	0.54(2)[b]	0.062(32)	$E2$
749.5(1)	1988.1	$13/2^- \rightarrow 11/2^-$	5.15(46)	1.41(18)[f]	−0.071(52)	$M1$
785.2(6)	2748.2	$17/2^+ \rightarrow 15/2^-$	27.0(15)	2.10(8)[g]	0.017(21)	$E1$
803.1(1)	2985.3	$21/2^+ \rightarrow 19/2^-$	12.91(95)	1.90(16)[c]	0.066(25)	$E1$
1141.8(1)	2713.8	$15/2^- \rightarrow 13/2^-$	11.98(81)	2.13(13)[e]	−0.032(25)	$M1$

[a]Relativeγ-ray intensities are estimated from prompt spectra and normalized to 100 for the total intensity of 319.0 keV γ rays.
[b]From the 785.2 keV ($E1$) DCO gate.
[c]From the 443.3 keV ($E2$) DCO gate.
[d]From the 803.1 keV ($E1$) DCO gate.
[e]From the 652.2 keV ($E2$) DCO gate.
[f]From the 319.0 keV ($M1+E2$) DCO gate.
[g]From the 724.3 keV ($E2$) DCO gate.

its measured DCO ratio, obtained using a quadrupole gate of 652 keV, and the positive Δ_{IPDCO} confirms it to be an $E2$ transition. The 443 keV γ ray was tentatively assigned as a mixed transition of $(M1+E2)$ type by Slocombe *et al.* [13]. It may be noted that there is a transition of energy 441 keV decaying from the 2883 keV level in the same band but is assigned as a mixed $M1+E2$ transition. Therefore, to avoid the possibility of contamination, the Δ_{IPDCO} of the 443 keV γ is obtained from the gate of 803 keV. On the other hand, the DCO ratio and Δ_{IPDCO} of 441 keV are obtained from the gate of 443 keV only, to avoid any contamination of 443 and 445 keV transitions. The presence of 161, 226, 230, 441, 504, 533, and 543 keV γ rays only in coincidence with the 427 keV and not with 803 keV is evident from the spectra of double

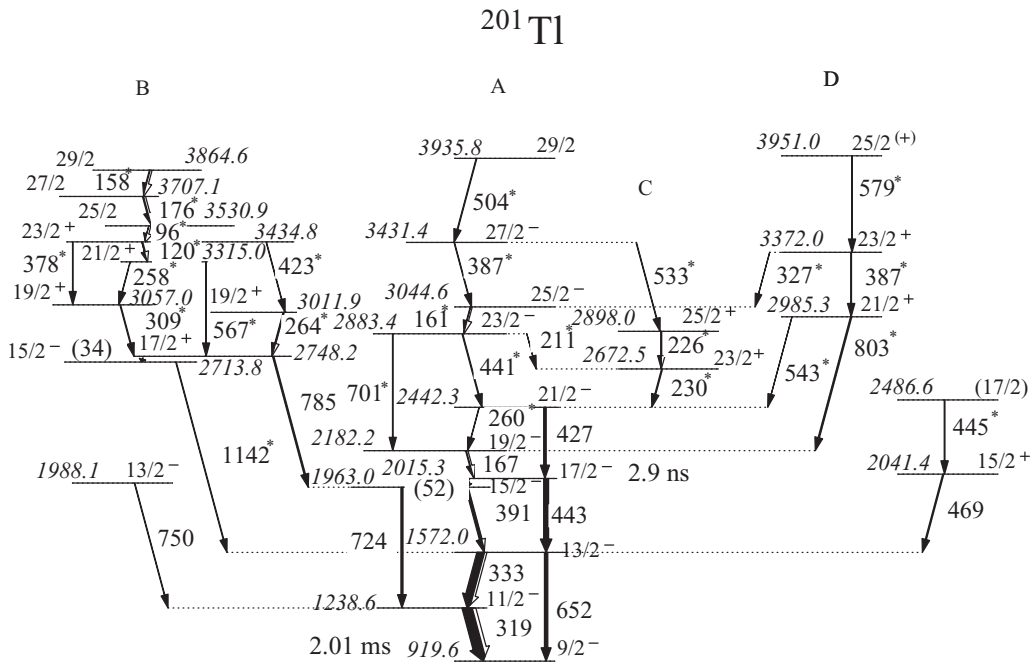

FIG. 8. Level scheme of ^{201}Tl above $9/2^-$ isomeric level, as obtained from the present work. New transitions are marked with "∗".

gates shown in Figs. 3(a) and 3(b). The 167 and 579 keV gamma rays, on the other hand, are in coincidence only with the 803 keV γ ray. This establishes the two separate cascade of γ rays connecting 427 and 803 keV.

The DCO ratio of the 803 keV γ ray is obtained from the gate of the known quadrupole transition of 652 keV, and along with the positive Δ_{IPDCO} confirms it as an $E1$ transition. The 387 keV transition has a double placement in the level scheme, one in band A and the other in band D [see Figs. 3(a) and 3(b)]. The DCO and Δ_{IPDCO} of the 387 keV transition, placed in band D, were obtained from the gate of 803 keV, which excludes any contribution of 387 keV transition of band A and turns out to be an $M1$ transition. The DCO ratio and Δ_{IPDCO} of the 387 keV of band A could not be obtained independently, as it is not in coincidence with any other strong transition, excluding the contribution of 387 keV of band D. Therefore, the spin-parity of the 3431 keV level of band A is fixed from the deduced multipolarity of the connecting transition of 533 keV to band C. The intensities of the two components of 387 keV belonging to bands A and D have been obtained from the gated spectrum of 161 and 803 keV transitions respectively with appropriate normalization. DCO ratios of the 161 and 167 keV transitions indicate that they are of mixed multipolarity and are considered to be $M1 + E2$ type. Polarization asymmetry cannot be obtained for 260, 327, 504, 543, 579, and 701 keV due to their poor statistics, but DCO ratios of the 504, 579, and 701 keV transitions attribute them as $M1/E1$, $(M1 + E2)$, and $E2$, respectively.

It may be noted that, other than the transitions tabulated in Table I, a few γ lines, viz., 102, 116, 148, and 853 keV, have also been observed in coincidence with all the transitions in ^{201}Tl placed in the level scheme. This can clearly be seen from the spectrum shown in Fig. 4, which is generated from the double gate of 148 and 853 keV γ rays. This spectrum suggests that the above γ rays must belong to ^{201}Tl. The fact that all the γ rays belonging to the bands A, B, and D are observed in the spectrum of Fig. 4, including the lower lying transitions of 724, 652, 319, and 333 keV, indicates that the above-mentioned unplaced transitions must be decaying to bands A, B, and D. The intensities of these transitions also support this fact. However, we have not observed a common higher energy level from which the bands A, B, and D are populated. Therefore, it is possible that this higher lying unobserved level is very close to all of the highest observed levels in different bands and connected to those bands by low energy, highly converted transitions. We did not get any evidence of such transitions connecting the three bands at the top because of not having the facility to detect low energy transitions or conversion electrons in our setup. Therefore, we constrain ourselves to place 102, 116, 148 and 853 KeV γ rays in the level scheme presented in Fig. 8. A more specific experiment with the aim to detect low energy transitions and conversion electrons would be required to resolve this issue.

IV. DISCUSSION

The proton and the neutron Fermi levels in ^{201}Tl lie just below the $Z = 82$ and $N = 126$ spherical shell closures, respectively. The shell model orbitals $3s_{1/2}$ and $2d_{3/2}$ are available for the odd proton, and the $h_{9/2}$ orbital (from above the $Z = 82$ magic gap) intrudes around the proton Fermi level, mostly for the deformed Tl nuclei. For neutrons, the available orbitals are $2f_{5/2}$, $3p_{3/2}$, and the unique parity high-j orbital $1i_{13/2}$. Low lying states in heavier odd-A Tl nuclei mostly originate due to the occupation of odd protons in the $3s_{1/2}$ or $2d_{3/2}$ orbitals as well as in the $1h_{11/2}$ orbital for medium excitation energy.

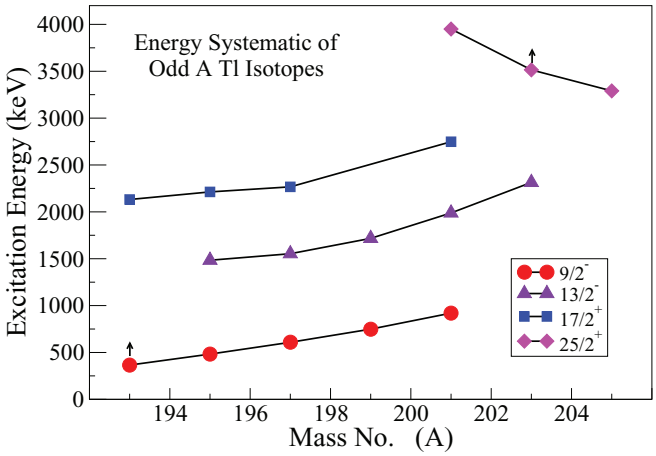

FIG. 9. (Color online) Energy systematic of the $9/2^-$, $13/2^-$, $17/2^+$, and $25/2^+$ states in odd-A thalium isotopes.

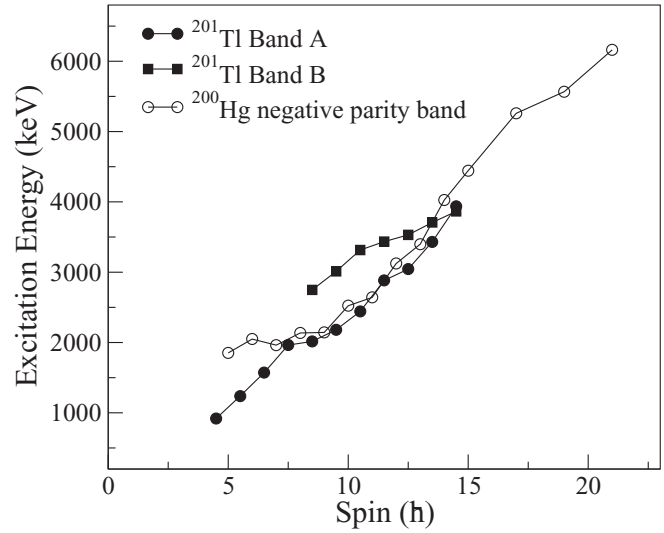

FIG. 10. Excitation energy as a function of spin for the bands A and B in ^{201}Tl and for the negative parity band in ^{200}Hg.

Apart from these levels a low-lying $9/2^-$ isomer has been reported in all the neutron deficient odd-A isotopes of Tl [6]. Rotational band structures based on this isomer have also been observed in the odd-A Tl isotopes in mass 180 and 190 regions. These were interpreted as oblate bands based on the [505]$9/2^-$ Nilsson orbital originating from the intruder $\pi h_{9/2}$ state. States in odd-A Tl isotopes are often described by the coupling of the odd proton in the $s_{1/2}$, $d_{3/2}$, and $h_{9/2}$ orbitals with the states in the neighboring even-even Hg core. Low-lying excited states in ^{201}Tl corresponding to the above single-particle states have been observed in an earlier study [13]. In the neighboring even-even nucleus ^{200}Hg, apart from the zero-quasiparticle ground state band, a band structure built on a 5^- state having the configuration of $\nu(p^{-1}_{3/2} \otimes i^{-1}_{13/2})$ [24] has been reported. The $13/2^-$ level at 1988 keV and the $17/2^+$ level at 2748 keV in ^{201}Tl are proposed to be due to the coupling of the $d_{3/2}$ and $h_{9/2}$ orbitals, respectively, with the above 5^- core state in ^{200}Hg.

The systematics of the excitation energies of these single- and multi-quasiparticle states in odd-A Tl isotopes is shown in Fig. 9. It can be seen from this figure that the trend of increasing energy of the $9/2^-$, $13/2^-$, and $17/2^+$ states with increase in neutron number continues up to ^{201}Tl. It can also be seen that the newly observed levels in ^{201}Tl in the present work nicely follow the systematic trend, supporting the proposed configuration. The gradual increase in energies of the multi-quasiparticle states is attributed to the increase in the single-particle energies, as shown for the $9/2^-$ level in the same figure. This increase in the excitation energy for the $9/2^-$ level can be interpreted from the fact that, as the neutron number increases towards the $N = 126$ shell closure, the deformation tends to decrease and the $h_{9/2}$ state becomes less and less accessible for the heavier Tl isotopes. For even higher neutron number this state is expected to become non-yrast and may not be observed. Indeed, the $9/2^-$ state has not been observed in ^{203}Tl [13]. In ^{199,201}Tl nuclei, the band structures built on the $9/2^-$ state were not well developed [13,25]. They were known only up to $15/2^-$ in ^{201}Tl [13] and up to $19/2^-$ in ^{199}Tl [25]. In contrast, the rotational band based on the $9/2^-$ isomer is known up to $29/2^-$ in the neighboring ^{197}Tl [7,14].

In the present work the band structure built on the $9/2^-$ isomer in ^{201}Tl (band A in Fig. 8) has been extended up to the $29/2$ state. Apart from this $9/2^-$ band, a band-like structure (band B) has also been observed in the present work built on the $17/2^+$ three-quasiparticle state. The excited state corresponding to the $\pi h_{11/2}$ excitation has been observed in some of the odd-A thalium isotopes. The state at 1414 keV with tentative spin of $(11/2)$, observed by Slocombe *etal*. [13] (not shown in the present level scheme), may correspond to the $\pi h_{11/2}$ state in ^{201}Tl. The corresponding three-quasiparticle state with a configuration of $\pi h^{-1}_{11/2} \otimes \nu(p^{-1}_{1/2} \otimes i^{-1}_{13/2})$ would be a state with $J^\pi = 25/2^+$ and has been observed in the heavier isotopes ^{203,205}Tl as an isomeric state [26,27]. A $(25/2^+)$ state has been observed in the present work at 3951 keV. The systematics of the excitation energy of this state is shown in Fig. 9. The systematic trends suggest that this state in ^{201}Tl may correspond to the above configuration.

The plots of excitation energy as a function of spin for bands A and B in ^{201}Tl are shown in Fig. 10 along with the negative parity (5^- band) band in the neighboring even-even core nucleus ^{200}Hg. Three different slopes observed in this figure for band A in ^{201}Tl clearly indicate three different configurations for this band at high spins. There is a remarkable similarity in these plots between band A in ^{201}Tl and the 5^- band in ^{200}Hg above a spin of about $8\hbar$, indicating the similar nature of the two bands at and above this spin. The band crossing in this band in ^{201}Tl will be discussed in the subsequent paragraphs. It can also be seen from Fig. 10 that band B in ^{201}Tl lies about 800 keV above the 5^- band in ^{200}Hg (for the lower lying levels) which is close to the excitation energy of the $\pi h_{9/2}$ state in ^{201}Tl. This supports our assumption of the configuration $\pi h_{9/2} \otimes \nu(p^{-1}_{3/2} \otimes i^{-1}_{13/2})_{5^-}$ for band B in ^{201}Tl.

It can also be seen from Fig. 10 that the positive parity band B seems to cross the $9/2^-$ negative parity band in ^{201}Tl at a spin value of about $I \geqslant 14.5\hbar$. Similar behavior has been reported in the lighter Tl isotope, ^{193}Tl [28], in which the positive parity band beyond the above spin becomes yrast. In comparison with

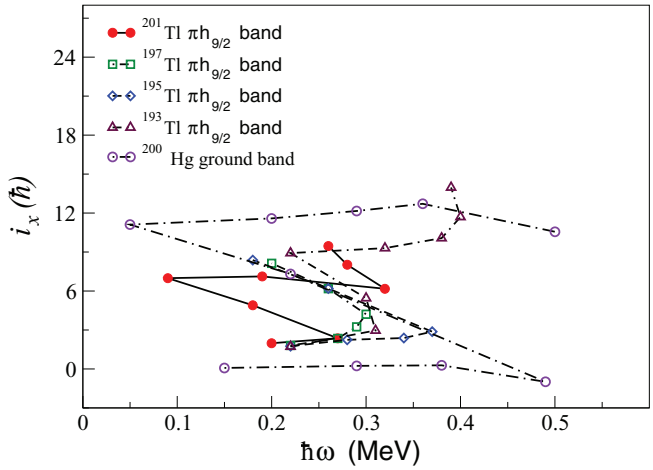

FIG. 11. (Color online) Alignment plot for the $\pi h_{9/2}$ bands in odd-A Tl isotopes. The same for the ground band in ^{200}Hg is also shown. The level energies of $h_{9/2}$ bands of $^{193-197}$Tl and ^{200}Hg are taken from Refs. [7,24,28] respectively.

the noncollective prolate structure in the neighboring ^{191}Hg nucleus [29,30], the positive parity states in ^{193}Tl at high spin were interpreted as single-particle states with the possibility of a noncollective prolate structure. In the case of ^{201}Tl, the positive parity states just begin to show similar behavior with a crossing point at exactly the same spin. Therefore, there is an indication of the appearance of a noncollective structure in ^{201}Tl similar to the ones observed in the lighter nuclei ^{193}Tl and ^{191}Hg. However, it is important to know the higher spin states in the positive parity band, which could not be observed in the present work, to draw a definite conclusion

The band crossing phenomena can be better visualized in the plot of aligned angular momentum, i_x, which is the projection of particle angular momentum onto the rotation axis. The plot of i_x as a function of rotational frequency is shown in Fig. 11 for the $\pi h_{9/2}$ bands in odd-A thalium isotopes along with that of the ground state band of the even-even ^{200}Hg. This figure shows that the first band crossing for the $\pi h_{9/2}$ band (band A) in ^{201}Tl occurs at a rotational frequency of $\hbar\omega \sim 0.27$ MeV. The gain in alignment after the first crossing is about $7\hbar$. The crossing frequency and the gain in alignment in ^{201}Tl are similar to those in the lighter isotopes of thalium as shown in this figure. The band crossings in the lighter thalium isotopes are attributed to the alignment of a pair of neutrons in the $i_{13/2}$ orbital. This seems to be the case for ^{201}Tl also. It may be noted that the gain in alignment for the ground state band in the neighboring even-even core nucleus ^{200}Hg (which is also interpreted as the alignment of a pair of neutrons in the $i_{13/2}$ orbital) is much higher at the first band crossing. Less gain in the aligned angular momentum for the odd-Z Tl nuclei indicates partial alignment in these nuclei.

The similarities in the alignment gain and frequencies show that the collective rotational nature of the $9/2^-$ state for the neutron-deficient thalium isotopes still persists for ^{201}Tl, for neutron number $N = 120$. After the band crossing, however, the levels become somewhat irregular and hence more spherical in nature. It can be seen from Fig. 11 that another band crossing at about $\hbar\omega \sim 0.33$ MeV seems to occur with a smaller gain in alignment, indicating the alignment of a pair of neutrons in $f_{5/2}$ and $p_{3/2}$ orbitals.

In the case of ^{200}Hg, it was observed by Andreas *et al.* [24] that the 5^- band (AE) is more yrast than the positive parity two-quasiparticle (AB) band which is the extension of the ground state band after the alignment of two neutrons in the $i_{13/2}$ orbital. This AB band decays more strongly to the AE band than to the ground band. It was argued that it is economical to rearrange one $i_{13/2}$ neutron hole to a $p_{3/2}$ state due to the closure of $i_{13/2}$ for $N = 120$, and hence there is more overlap between the AB band and the AE band [24]. Therefore, the AB band decays to the AE band by a strong $E1$ transition. In the case of ^{201}Tl, the $17/2^+$ state in band B decays to the $15/2^-$ state, just around the band crossing region in band A, by a strong $E1$ transition. Also the $9/2^-$ band becomes weaker after the alignment of two neutrons in the $i_{13/2}$ orbital, as in the case of the ground band in ^{200}Hg. These observations suggest that the above argument in Ref. [24] is valid in the case of the odd-$AN = 120$ isotone ^{201}Tl also. The presence of the negative parity orbitals ($p_{3/2}$ and $f_{5/2}$) above the closed $i_{13/2}$ positive parity orbital for the neutrons explains the occurrence of several $E1$ transitions in the level scheme of ^{201}Tl, observed in the present work, from the states at moderate excitation energy where three and five quasiparticle states are expected.

V. TRS CALCULATIONS

In order to study the deformation in ^{201}Tl, the total Routhian surface (TRS) calculations are performed by the Strutinsky shell correction method using a deformed Woods-Saxon potential with BCS pairing for the calculation of the single-particle shell energies [31,32]. The universal parameter set was used for the calculations. The Routhian energies were calculated in $(\beta_2, \gamma, \beta_4)$ deformation mesh points with minimization on β_4. The procedure of such calculations has been outlined in Ref. [33]. The Routhian surfaces are plotted in the conventional β_2-γ plane. The TRSs are calculated for different values of rotational frequencies $\hbar\omega$ and for different configurations. At each frequency, the spin can be projected. The TRSs calculated for the negative parity $h_{9/2}$ configuration are shown in Fig. 12 for $\hbar\omega = 0.16, 0.31$, and 0.36 MeV. These values of rotational frequencies correspond to the situation before and after the alignments in the $h_{9/2}$ band.

It can be seen that a minimum in the TRS is obtained at an oblate deformation with $\beta_2 = 0.10$ for $\hbar\omega = 0.16$ MeV, i.e., for the low-lying states below any particle alignment. The calculations for the lighter odd-A isotopes ^{193,197,199}Tl show somewhat larger deformation of $\beta_2 = 0.15$ for the same configuration. Therefore, the deformation decreases with the increase in neutron number for the Tl isotopes, as expected, and as has been reflected in the increase in the excitation energy of the $h_{9/2}$ state in the Tl isotopes as a function of neutron number (see Fig. 9). It can also be seen that, as the rotational frequency increases, the deformation gradually decreases and the TRS for $\hbar\omega = 0.36$ MeV [Fig. 12(a)] shows that there is no minimum at the oblate shape and the deformation is close to

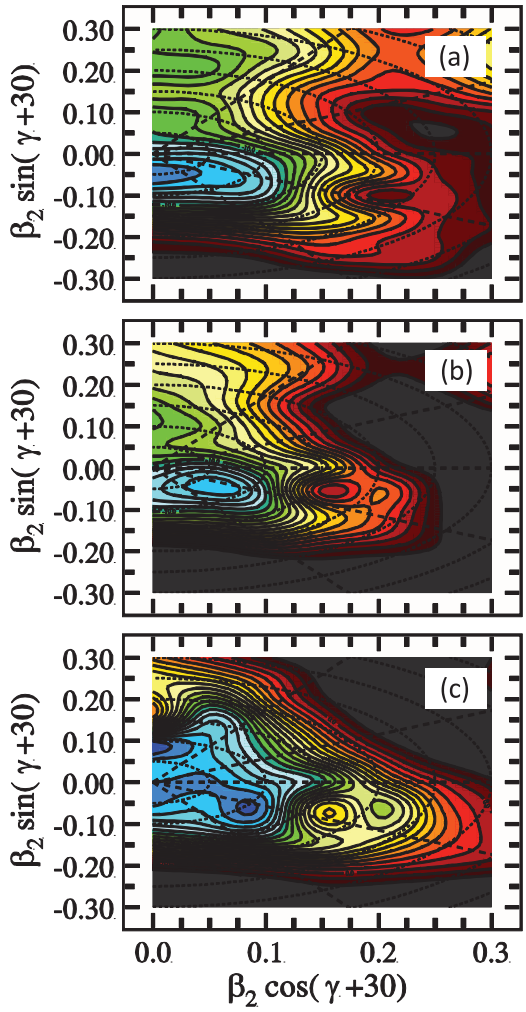

FIG. 12. (Color online) Total Routhian surface (TRS) calculations for band A in ^{201}Tl for rotational frequency $\hbar\omega =$ (a) 0.36 MeV, (b) 0.31 MeV, and (c) 0.16 MeV.

$\beta_2 \sim 0$. Therefore, the single-particle-like structure observed at higher excitation energy in the level scheme of ^{201}Tl is consistent with the TRS calculations.

VI. CONCLUSION

High spin states in ^{201}Tl have been populated by using the fusion evaporation reaction ^{198}Pt(^{7}Li,4n) at a beam energy of 45 MeV and studied by γ-ray coincidence spectroscopic techniques using the INGA setup of 15 clover HPGe detectors. The level scheme of ^{201}Tl has been extended considerably up to an excitation energy of $\sim$ 3.9 MeV and spin of $29/2\hbar$ through the observation of 31 new transitions. The spin and parity assignments were done by DCO and IPDCO measurements. High spin states in ^{201}Tl have been compared with other Tl isotopes and also with the core nucleus ^{200}Hg. The observation of a rotation-like structure for the $h_{9/2}$ band suggests that the deformed structure still persists in the Tl isotopes for neutron number $N = 120$. It was shown that the experimental observations are consistent with the total Routhian surface (TRS) calculations which predict oblate deformed shape for the low lying states in the $h_{9/2}$ configuration with $\beta_2 = 0.10$, and the deformation gradually decreases with the increase in rotational frequency. The calculations also show that the deformation in ^{201}Tl is less than that in the lighter isotopes. Apart from the $h_{9/2}$ band, other states resulting from the coupling of the low-lying odd-proton states with the two-neutron state (5^-) in the ^{200}Hg core have also been identified in the present work. The excitation energies of these states are found to be consistent with the systematic of the odd-A thalium isotopes. An indication of the appearance of noncollective positive parity states being yrast above spin $I \geqslant 29/2\hbar$, similar to ^{193}Tl, has been observed for ^{201}Tl in the present work. However, higher spin states in the positive parity band need to be explored in this nucleus for confirmation.

ACKNOWLEDGMENTS

The authors would like to thank all members of the INGA collaboration for setting up of the clover HPGe array at TIFR, Mumbai. The untiring efforts of the staff of the BARC-TIFR Pelletron LINAC facility at Mumbai to provide a good quality beam are gratefully acknowledged. Special thanks are due to Prof. R. G. Pillay of TIFR, Mumbai for his guidance, encouragement, and stimulating discussions during the experiment.

[1] A. Covello and G. Sartoris, Nucl. Phys. A **93**, 481 (1967).
[2] I. Hamamoto, Phys. Rep. **10**, 63 (1974).
[3] K. Heyde, P. Van Isacker, M. Waroquier, J. L. Wood, and R. A. Meyer, Phys. Rep. **102**, 291 (1983).
[4] W. Reviol, L. L. Riedinger, J. M. Lewis, W. F. Mueller, C. R. Bingham, J. Y. Zhang, and B. E. Zimmerman, Phys. Scr. **T56**, 167 (1995).
[5] J. O. Newton, S. D. Cirilov, F. S. Stephens, and R. M. Diamond, Nucl. Phys. A **148**, 593 (1970).
[6] J. O. Newton, F. S. Stephens, and R. M. Diamond, Nucl. Phys. A **236**, 225 (1974).
[7] R. M. Lieder, A. Neskakis, M. Müller-Veggian, Y. Gono, C. Mayer-Böricke, S. Beshai, K. Fransson, C. G. Linden, and Th. Lindblad, Nucl. Phys. A **299**, 255 (1978).
[8] S. Pilotte *et al.*, Phys. Rev C **49**, 718 (1994).
[9] P. B. Fernandez *et al.*, Nucl. Phys. A **517**, 386 (1990).
[10] F. Azaiez *et al.*, Z. Phys. A **338**, 471 (1991).
[11] J. Wrzesiński *et al.*, Eur. Phys. J. A **20**, 57 (2004).
[12] R. M. Diamond and F. S. Stephens, Nucl. Phys. A **45**, 632 (1963).
[13] M. G. Slocombe, J. O. Newton, and G. D. Dracoulis, Nucl. Phys. A **275**, 166 (1977).
[14] H. Pai *et al.*, arXiv:1307.2056.
[15] A. Srivastava *et al.*, Phys. Lett. B **718**, 931 (2013).
[16] R. Palit *et al.*, Nucl. Instrum. Methods Phys. Res. A **680**, 90 (2012).
[17] D. C. Radford, Nucl. Instrum. Methods Phys. Res. A **361**, 297 (1995).

[18] R. K. Bhowmik, S. Muralithar, and R. P. Singh, Proceedings of the DAE Symposium on Nuclear Physics, 2001, Vol. 44B (unpublished), p. 422.
[19] A. Krämer-Flecken, T. Morek, R. M. Lieder, W. Gast, G. Hebbinghaus, H. M. Jäger, and W. Urban, Nucl. Instrum. Methods Phys. Res. A **275**, 333 (1989).
[20] K. Starosta *et al*., Nucl. Instrum. Methods Phys. Res. A **423**, 16 (1999).
[21] Ch. Droste, S. G. Rohoziński, K. Starosta, T. Morek, J. Srebrny, and P. Magierski, Nucl. Instrum. Methods Phys. Res. A **378**, 518 (1996).
[22] H. Pai *et al*., Phys. Rev. C **85**, 064313 (2012).
[23] J. M. Blatt and V. F. Weisskopf, *Theoretical Nuclear Physics* (Wiley, New York, 1956), pp. 623–628.
[24] A. Görgen *et al*., Eur. Phys. J. A **6**, 141 (1999).
[25] N. Marginean *et al*., Eur. Phys. J. A **46**, 329 (2010).
[26] M. Pfützner *et al*., Phys. Lett. B **444**, 32 (1998).
[27] J. A. Becker *et al*., Phys. Rev. C **29**, 1268 (1984).
[28] W. Reviol *et al*., Nucl. Phys. A **548**, 331 (1992).
[29] D. Ye *et al*., Nucl. Phys. A **537**, 207 (1992).
[30] T. Bengtsson and I. Ragnarsson, Nucl. Phys. A **436**, 14 (1985).
[31] W. Nazarewicz, J. Dudek, R. Bengtsson, T. Bengtsson, and I. Ragnarsson, Nucl. Phys. A **435**, 397 (1985).
[32] W. Nazarewicz, M. A. Riley, and J. D. Garrett, Nucl. Phys. A **512**, 61 (1990).
[33] G. Mukherjee, P. Joshi, R.K. Bhowmik, S. N. Roy, S. Dutta, S. Muralithar, and R. P. Singh, Nucl. Phys. A **829**, 137 (2009).